Cell Reports, Volume *28*

Supplemental Information

White Matter Network Architecture Guides Direct Electrical Stimulation through Optimal State Transitions

Jennifer Stiso, Ankit N. Khambhati, Tommaso Menara, Ari E. Kahn, Joel M. Stein, Sandihitsu R. Das, Richard Gorniak, Joseph Tracy, Brian Litt, Kathryn A. Davis, Fabio Pasqualetti, Timothy H. Lucas, and Danielle S. Bassett

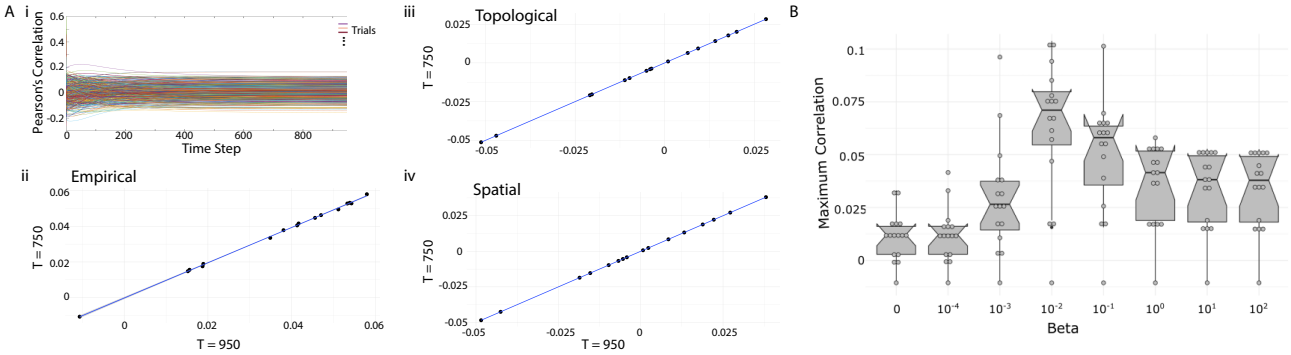

Figure S1: Related to Figure 2 in the main text. ***Effects of Different Parameter Choices in Open Loop Control.*** **A: Effect of the Number of Time Steps Used**: (*i*) For a representative subject, correlation coefficients between the empirical post-stimulation state and the simulated state for every time step in the simulation. Colored lines represent different trials. (*ii*) The maximum correlation coefficient values for empirical white matter connectivity for every subject when simulations were run with two different numbers of time steps: 750 time steps and 950 time steps. (*iii, iv*) Here we show the results of performing the same analysis displayed in panel (*ii*) but for topological and spatial null models. **B: The effect of the scaling parameter β on the correlations observed between the true post-stimulation state and the predicted post-stimulation state.** Here we show the maximum correlations reached as a function of the β value used in the model. In the main manuscript, we report results for $\beta = 1$, while here in the supplement we report qualitatively similar results for $\beta = 0.1$. We first observe that empirical graphs reach a maximum correlation that is significantly different from zero ($N = 11$, t-test $t = 5.07$, $p = 4.83 \times 10^{-4}$). In the topological null model, we observe smaller maximum correlations (paired t-test: $N = 11$, $t = 4.76$, $p = 7.64 \times 10^{-4}$), and earlier peaks ($N = 11$, $t = 7.40$, $p = 2.33 \times 10^{-5}$). Similarly in the spatial null model, we observe smaller maximum correlations ($N = 11$, $t = 4.10$, $p = 2.15 \times 10^{-3}$), and earlier peaks ($N = 11$, $t = 3.41$, $p = 6.70 \times 10^{-3}$).

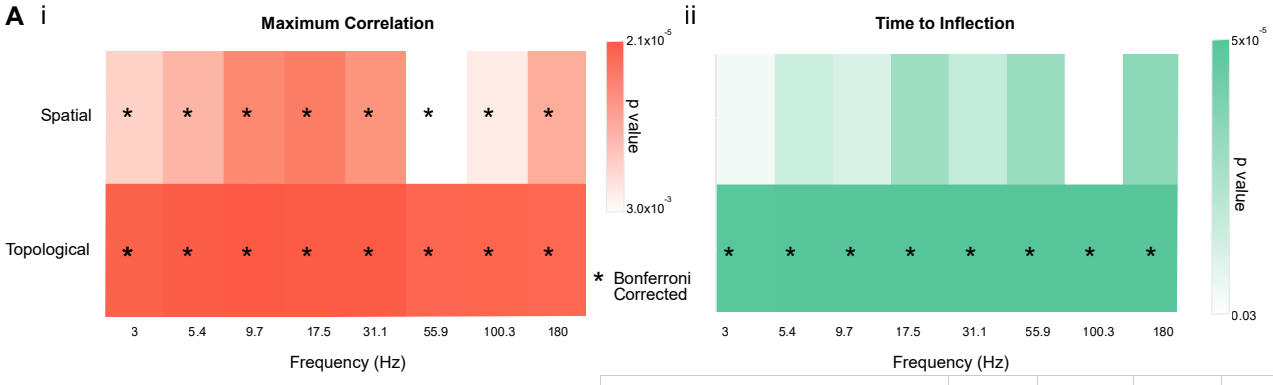

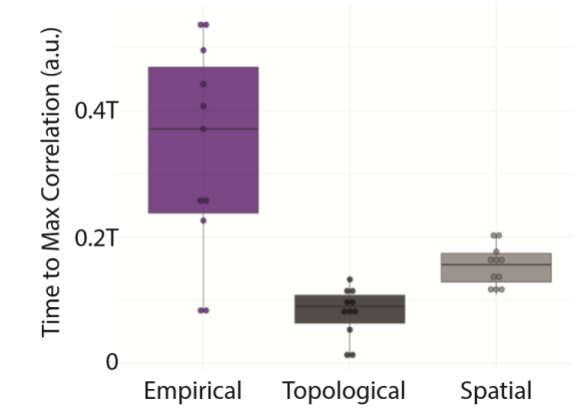

C

Alternate Atlas (*N* = 463)				
Test	***N* subjects**	***F/t* value**	***p* value**	
repeated measures ANOVA	11	*F(2,20)* = 18	3.3×10^{-5}	
one sample *t*-test for empirical correlations	11	*t* = 4.9	6.05×10^{-4}	
paired t-test: empirical vs topological correlation	11	*t* = 4.4	1.34×10^{-3}	
paired t-test: empirical vs spatial correlation	11	*t = 4.2*	1.19×10^{-3}	
paired t-test: empirical vs topological peak time	11	*t = 8.67*	5.76×10^{-6}	
paired t-test: empirical vs spatial peak time	11	*t = 2.64*	0.025	
Within Subject Analyses				
Test	***N* trials**	***d* value**	***p* value**	**number of datasets**
KS test: empirical vs topological correlations	> 192	> 0.63	$< 6.02 \times 10^{-6}$	10/16
KS test: empirical vs spatial correlations	> 192	> 0.5	$< 1.3 \times 10^{-3}$	9/16
KS test: empirical vs topological peak times	> 192	> 0.71	$< 1.1 \times 10^{-6}$	15/16
KS test: empirical vs spatial peak times	> 192	> 0.53	$< 8.9 \times 10^{-8}$	8/16

Figure S2: Related to Figure 2 in the main text. ***Alternative Ways to Operationalize Brain States and Dynamic Properties*** **A: Results for simulations in which brain state represents power in single frequency bands.** *(i)* Results for paired t-tests comparing the maximum correlation observed between the true post-stimulation state and the predicted post-stimulation state, for the spatial null model (*top*) and the topological null model (*bottom*) for each of the 8 frequency bands (*x-axis*). *(ii)* Results for paired t-tests comparing the time to inflection for the spatial null model (*top*) and the topological null model (*bottom*) for each of the 8 frequency bands (*x-axis*). In both panels *(A)* and *(B)*, we display the associated p-values in the color of each square; values that pass Bonferroni correction for multiple comparisons are indicated with an asterisk. **B: Time to Maximum (rather than peak) Correlation**: Box plots depicting the average time to reach the maximum correlation between the empirically observed post-stimulation state and the predicted post-stimulation state at every time point in the simulated trajectory $x(t)$. Box plots indicate the median and quartiles of the data. We find a main effect for graph type (repeated measures ANOVA $F(2, 20) = 21.84$, $p = 9.34 \times 10^{-6}$). We also find that the empirical networks peak significantly later than both the topological (paired t-test: $N = 11$, $t = 5.82$, $p = 1.69 \times 10^{-4}$) and spatial (paired t-test: $N = 11$, $t = 3.49$, $p = 5.79 \times 10^{-3}$) null models. **C: Statistics for alternate atlas and within subject analyses**: All analyses from the main text were replicated when using a smaller parcellation of the Lausanne ($N = 463$) atlas. Analyses from the main text were also repeated within each dataset (subject and stimulation site combination) and across trials. The table gives the minimum number of trials in the test, an effect size threshold, a p-value threshold, and the number of datasets with larger effect sizes and smaller p-values than the given thresholds.

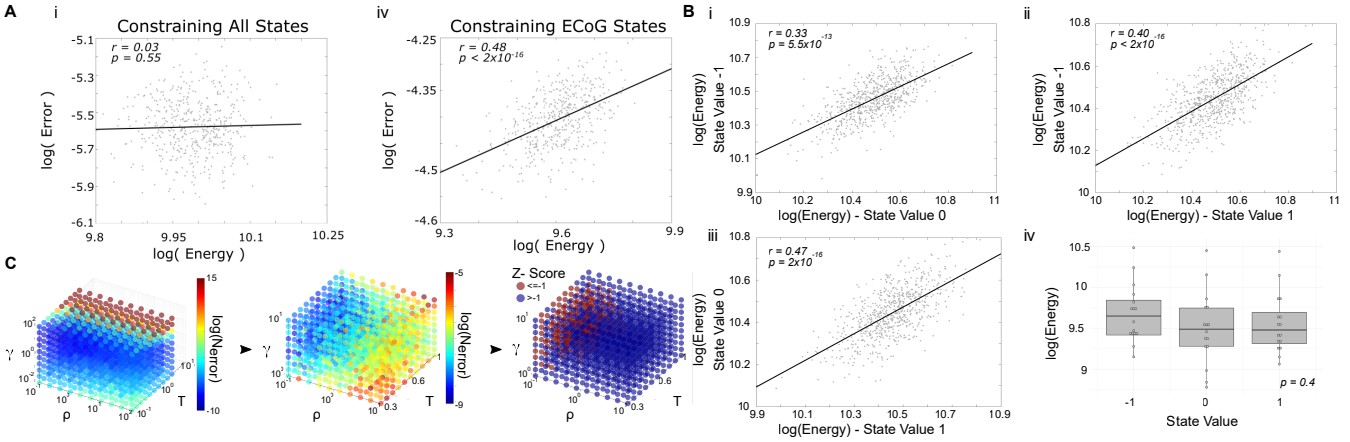

Figure S3: Related to Figures 3-6 in the main text. ***Robustness and Selection of Parameters for Optimal Control*** **A: Impact of the Choice of S on the Relation Between Energy and Error.** When **S** is the identity matrix, none of the 16 data sets showed a significant correlation between energy and error. *(i)* For one representative subject, we show the scatterplot of log(energy) versus log(error) when **S** is the identity matrix. At the single-subject level, we observed that when **S** contains zeros along the diagonal at ROIs without electrodes present (and thus only constrains the states of regions with ECoG electrodes), then 13 of the 16 data sets displayed a significant correlation between energy and error (Bonferroni corrected $p < 0.003$). *(ii)* For the same subject, we show the scatterplot of log(energy) versus log(error) when **S** is selected to only constrain the states of regions with ECoG electrodes in them. Based on these findings, we selected **S** to be the identity matrix. **B: Impact of Initial State Value on the Relation Between Energy and Error.** We test whether these state values change the relative energies between trials within individuals by calculating the Pearson's correlation coefficient between the energy from all possible pairs of state values. We find that all subjects showed highly significant correlations between results obtained with the 0 state value and results obtained with the 1 state value, as well as highly significant correlations between results obtained with the 0 state value and results obtained with the -1 state value, after Bonferroni correction for multiple comparisons ($p < 0.001$). Fourteen out of 16 data sets showed significant correlations between results obtained with the -1 state value and results obtained with the 1 state value. *(i)* For one representative subject, we show the scatterplot of log(energy) when the state value was set to -1, versus when it was set to 0. *(ii)* For the same subject, we also show the scatterplot of log(energy) when the state value was set to -1, versus when it was set to 1. *iii* For the same subject, we show the scatterplot of log(energy) when the state value was set to 0, versus when it was set to 1. We next tested whether the average magnitude of the energy for each state value was different across subjects. A one-way ANOVA returned no significant differences across state values ($F(2, 45) = 0.93, p = 0.40$) *(iv)* The average energy for each dataset for all state values (-1, 0, 1). **C: Method for Parameter Selection.** We began by calculating the error values of the simulations for every subject for each value of ρ, γ, and T. After selecting a range with small enough error (left-center), error values are z-scored to select only parameter combinations with a z-score less than -1 (center-right). The center coordinate from this latter space was selected to dictate the final parameter choice values: $\gamma = 4$, $T = 0.7$, and $\rho = 0.3$.

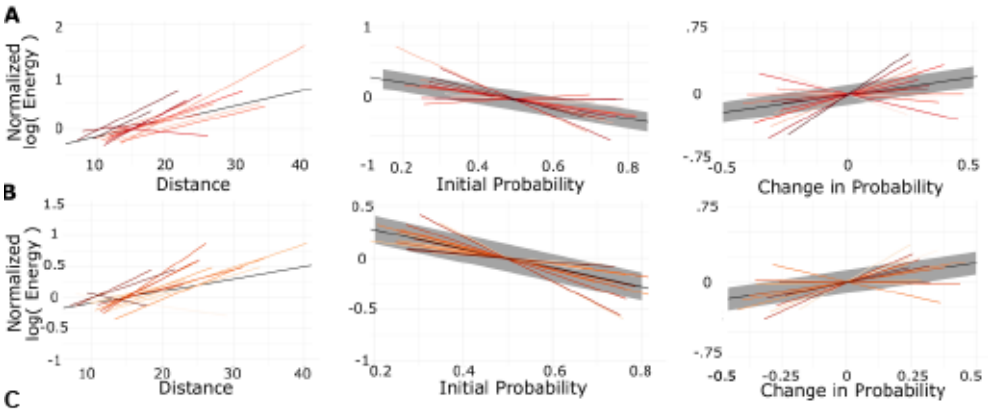

Alternate Optimal Control Parameters		
Test	***N***	***p value***
linear mixed effects model: Frobenius norm distance	7547	< 2x10-16
linear mixed effects model: initial probability	7547	< 2x10-16
linear mixed effects model: change in probability	7547	<6.9x10-15

Figure S4: Related to Figure 3 in the main text. **Relationships Between Energy and Distance in Topological and Spatial Null Models.** ***A*** Relationship between distance and energy for simulations using topological null

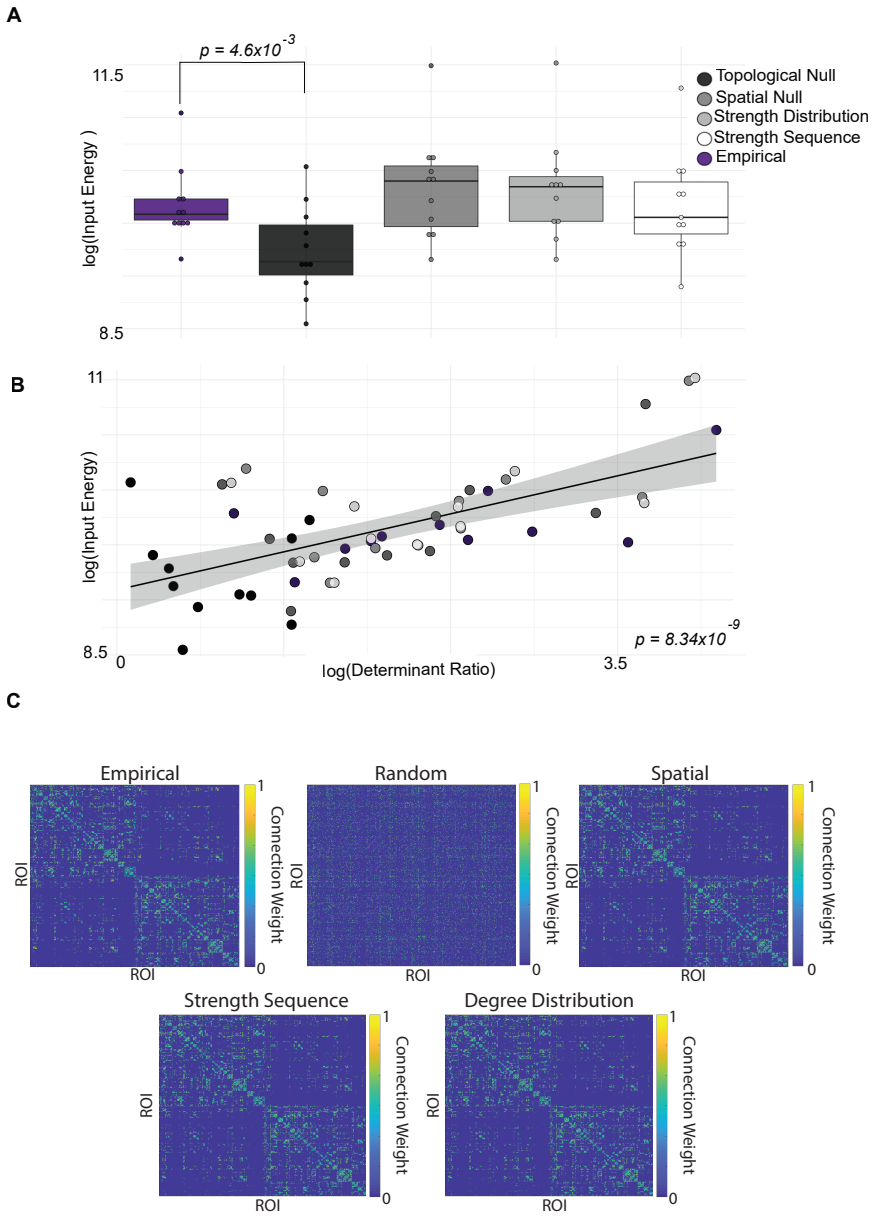

Figure S5: Related to Figure 4 (and Figure 2 for part **B**) in the main text. ***Additional Spatially Embedded Null Models.*** **(A: Effects on Average Energy Requirements)** Before exploring the energy used by different graph models, it is important to note that the numerical error returned for every network was consistently less than 0.004, indicating that the trajectories were highly accurate. Across graph types, we found a significant difference in the energy required for the transition from the initial state to the good memory state (repeated measures ANOVA $F(4, 40) = 12.96$, $p = 7.42 \times 10^{-7}$). In *post-hoc* analyses, we observed that neither of the additional null models were significantly different from those observed in the empirical graphs (paired t-test for weight preserving: $N = 11$, $t = 0.071$, $p = 0.945$; strength sequence preserving: $N = 11$, $t = -1.71$, $p = 0.12$). Average energy required for each transition from the pre-stimulation state to a good memory state, as theoretically predicted from Eq. 1 where **A** is (i) the empirical networks (purple) estimated from the diffusion imaging data, (ii) the topological null model graphs (black), (iii) the spatial null model graphs (dark charcoal), (iv) the spatial strength distribution preserving null model graphs (medium charcoal), and (v) the spatial strength sequence preserving null model graphs (white). **B: The relationship between the determinant ratio and the energy required for the transition from the pre-stimulation state to a good memory state.** Additionally, across all graphs, we still observe a significant relationship between energy and the determinant ratio (linear mixed effects model $N = 11$, $\chi^2 = 33.2$, $p = 8.34 \times 10^{-9}$). Note: The color scheme is identical to that used in panel *(A)*.**C: Visualization of Null Models.** Visualizations of empirical connectivity matrices (top left) and all null models (random, spatial, strength sequence preserving, and degree distribution preserving). Color bar gives the connection weight (QA).

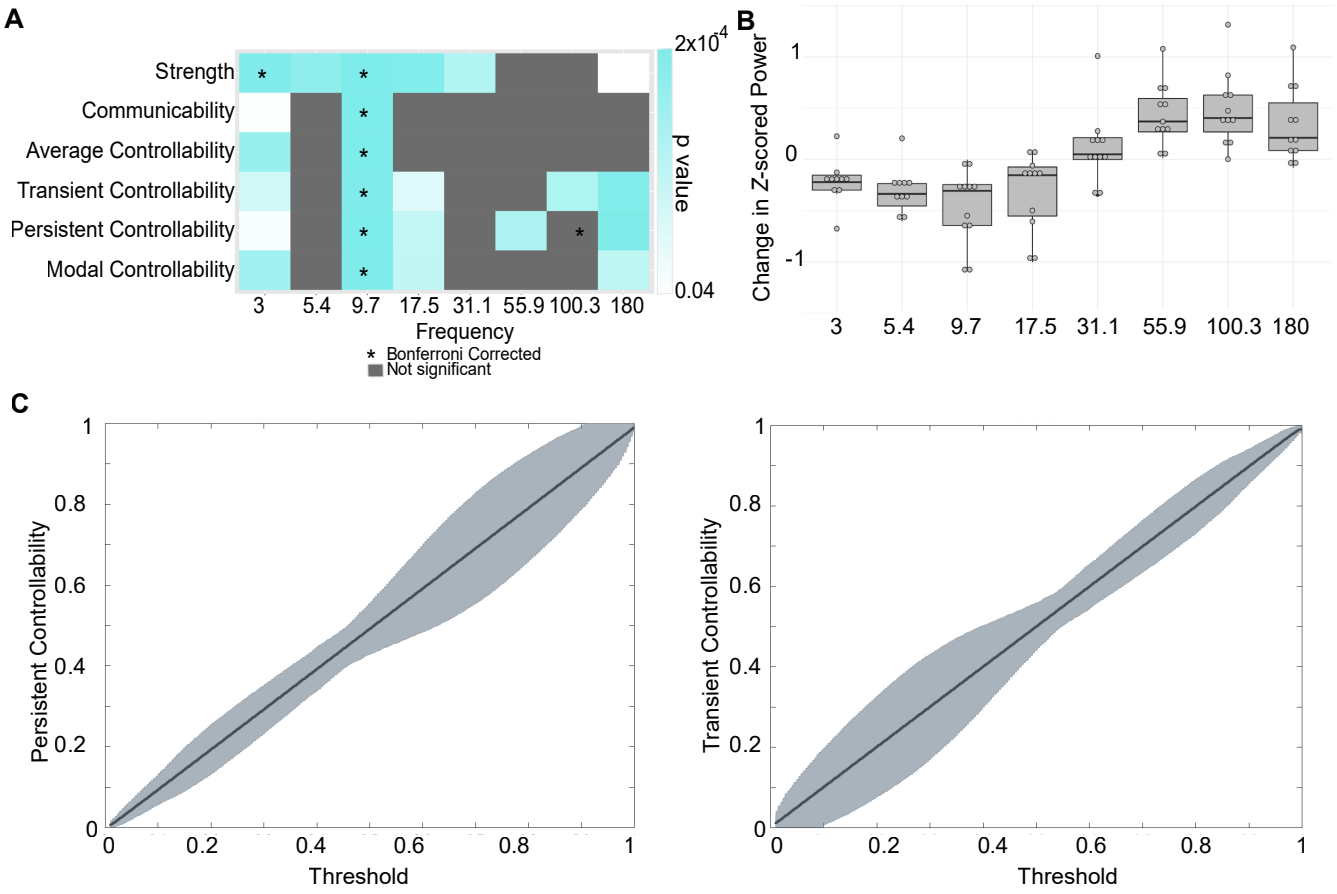

Figure S6: Related to Figure 5 in the main text. ***Additional Analyses Related to Regional Topology.*** **A: Additional Control Metrics Associated With Energy in the Alpha Band.** A heat map of the significance of the relationship between each regional metric and input energy (estimated with a linear mixed effects model) for each frequency band. **B: Change in Power Across Different Bands** The average difference in power between all initial states and target state for each frequency band. Note: the alpha band does not show strikingly greater difference, suggesting that the finding that all metrics are significant in the alpha band is not due to a difference in the magnitude of the transition. **C: Persistent and Transient Modal Controllability.** To select a cut-off for persistent and transient modal controllability calculations, we plotted the persistent *(Left)* and transient *(Right)* controllability value for every node as a function of threshold on the eigenvalues of the adjacency matrix **A**. Here we show the mean (black) and standard deviation across nodes (grey) from one representative, and randomly chosen, subject. A threshold of 10% was chosen as a value that would provide sufficient variance and measure a small number of modes.

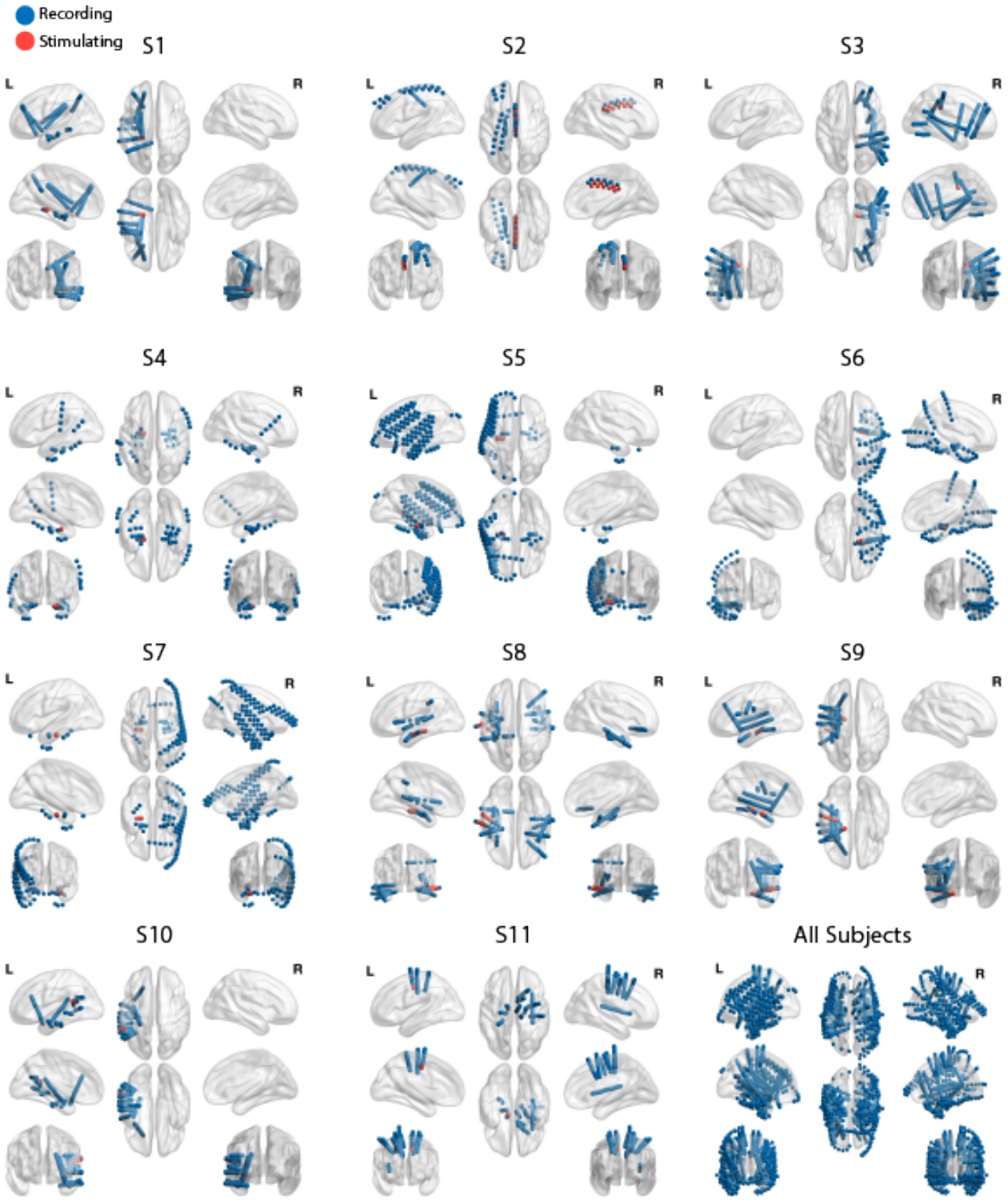

Figure S7: Related to the STAR Methods: Experimental Model and Subject Details. **Electrode Coverage:** Visualization of each subject's electrodes mapped to MNI space. Blue electrodes were only used for recording; red electrodes were used for stimulation.

A

Subject	Age at Implant	Gender	Handedness	Years of Education	Number of electrodes	Unique Stimulation Bipolar Pair ROIs	Stim Sessions
1	23	Male	Left	16	109	LH_hyppocampus	1
2	24	Female	Right	12	59	RH_hyppocampus	1
3	23	Female	Right	12	146	RH_isthmuscingulate, RH_precuneus	1
4	39	Male	Right	16	46	LH_entorhinal, LH_hyppocampus	1
5	45	Female	Right		127	LH_hyppocampus	1
6	39	Female	Ambidextrous	16	75	RH_hyppocampus	1
7	36	Male	Left		128	LH_hyppocampus, LH_parahippocampal	1
8	40	Female	Right	16	109	LH_middletemporal, LH_fusiform, LH_inferiortemporal	3
9	49	Female	Right	12	101	LH_hyppocampus , LH_fusiform, LH_middletemporal, LH_amygdala	2
10	20	Male	Right	12	97	LH_bankssts, LH_superiortemporal	2
11	18	Female	Right	12	109	LH_superiorfrontal	1

B

Subject	Unique ROIs with Elecs
1	LH_amygdala', 'LH_bankssts', 'LH_caudate' ,'LH_fusiform', 'LH_hyppocampus', 'LH_inferiorparietal' ,'LH_inferiortemporal', 'LH_insula', 'LH_isthmuscingulate',
2	LH_caudalmiddlefrontal', 'LH_inferiorparieta ', 'LH_paracentral', 'LH_postcentral ', 'LH_posteriorcingulate', 'LH_precentral', 'LH_rostralmiddlefrontal', 'LH_superiorfrontal ',
3	RH_amygdala ', 'RH_bankssts ', 'RH_caudalmiddlefrontal ', 'RH_caudate', 'RH_fusiform', 'RH_hyppocampus', 'RH_inferiorparietal', 'RH_insula', 'RH_isthmuscingulate', 'RH_lateraloccipital ', 'RH_lateralorbitofrontal', 'RH_lingual', 'RH_medialorbitofrontal',
4	RH_amygdala', 'RH_bankssts', 'RH_caudalmiddlefrontal ', 'RH_caudate ', 'RH_fusiform', 'RH_hyppocampus', 'RH_inferiorparietal ', 'RH_insula', 'RH_isthmuscingulate ', 'RH_lateraloccipital', 'RH_lateralorbitofrontal', 'RH_lingual ', 'RH_medialorbitofrontal',
5	LH_bankssts', 'LH_caudalmiddlefrontal ', 'LH_frontalpole', 'LH_fusiform ', 'LH_hyppocampus', 'LH_inferiorparietal ', 'LH_inferiortemporal ', 'LH_lateralorbitofrontal', 'LH_medialorbitofrontal', 'LH_middletemporal ',
6	LH_brainstem ', 'RH_amygdala', 'RH_fusiform', 'RH_hyppocampus ', 'RH_inferiorparietal', 'RH_inferiortemporal', 'RH_insula', 'RH_lateraloccipital',
7	LH_amygdala', 'LH_fusiform', 'LH_hyppocampus ', 'LH_medialorbitofrontal', 'LH_parahippocampal', 'RH_amygdala', 'RH_bankssts', 'RH_entorhinal ', 'RH_fusiform ', 'RH_hyppocampus', 'RH_inferiorparietal', 'RH_inferiortemporal ',
8	LH_amygdala', 'LH_fusiform', 'LH_hyppocampus', 'LH_inferiortemporal', 'LH_insula', 'LH_isthmuscingulate', 'LH_middletemporal ', 'LH_paracentral', 'LH_posteriorcingulate', 'LH_putamen', 'LH_superiorparietal', 'LH_superiortemporal', 'LH_supramargina',
9	LH_amygdala', 'LH_bankssts', 'LH_caudalmiddlefrontal', 'LH_caudate', 'LH_fusiform', 'LH_hyppocampus ', 'LH_inferiortemporal', 'LH_insula', 'LH_middletemporal',
10	LH_bankssts ', 'LH_caudate ', 'LH_fusiform', 'LH_inferiorparietal', 'LH_inferiortemporal', 'LH_insula', 'LH_middletemporal', 'LH_parahippocampal', 'LH_parstriangularis',
11	LH_paracentral', 'LH_postcentral', 'LH_posteriorcingulate', 'LH_precentral', 'LH_superiorfrontal', 'RH_caudalanteriorcingulate', 'RH_caudalmiddlefrontal',

Table S1: Related to the STAR Methods: Experimental Model and Subject Details. **A: Subject Information.** Demographic and task relevant information about each subject. Stimulation locations are given as unique regions in which either the anode or cathode were located. Stimulation sessions refers to the number of times that the task was run. Each session utilitized a different set of stimulation electrodes. **B: Subject Coverage.** More detailed information about the coverage of electrodes for each subject. Lists are of unique regions in which each subject had electrodes present. LH and RH indicate the hemisphere (left or right).